On Jupiter's atmospheric dynamics after the impact of comet P/Shoemaker-Levy 9

Joseph Harrington, Raymond Paul LeBeau, Jr., Kari A. Backes,

and Timothy E. Dowling

Massachusetts Institute of Technology, 77 Massachusetts Avenue,

Cambridge, Massachusetts 02139, USA

Submitted to *Nature* 12 December 1993.

Revision 3.5, 8 February 1994.

Manuscript: H12698 KZ/rl

OVER **20 fragments of comet P/Shoemaker-Levy 9 will collide with Jupiter on 18–24 July 1994[1–3]. If detectable, inertia-gravity waves emanating from the impacts will constitute an ideal experiment to learn about the atmosphere's stratification. We have simulated the event using a global, multi-layer model of Jupiter's atmosphere, and find inertia-gravity waves with temperature perturbations of 0.004–1.2 K resulting from energy deposition in the expected range of 10^{27}–10^{30} ergs. Thermal infrared images may reveal a temperature signature from the larger impacts, and visible-light images may show changes in cloud condensation patterns. Even weak signals may be detectable because the waves propagate in coherent rings centered on the impact point. Simulations indicate that a small vortex results from each impact, but that the vortex is sheared apart by the zonal winds within a few weeks.**

An atmosphere's density stratification, the rate at which density decreases with altitude, strongly influences the type of weather it exhibits. On Jupiter, stratification is poorly constrained in the most active region of the atmosphere, the troposphere. The deformation radius, L_d, is one measure of stratification. For length scales smaller than L_d, gravity flattens pressure highs and lows; for length scales larger than L_d, the Coriolis force sustains these anomalies. On Jupiter, L_d

ranges from ∼3,000 km in the stratosphere[4] to zero in the neutrally-stable convecting interior. Observational data poorly constrain the transition between these extremes, yet the transition greatly affects tropospheric meteorology. For example, the effective L_d in two-layer atmosphere models[5–8] is uncertain by a factor of 5, and since L_d is usually squared in fluid equations, key dynamical terms are uncertain by a factor of 25.

One can determine L_d by measuring the speed of inertia-gravity waves. These waves are generated by the adjustment process that brings large-scale disturbances into geostrophic balance. The group velocity of the leading wavefront is $c \sim L_d f$, where $f = 2\Omega \sin(\lambda)$ is the Coriolis parameter, Ω is the planetary rotation rate, and λ is planetographic latitude. The Shoemaker-Levy 9 impacts may provide the needed perturbations to set observable waves in motion, after which their speeds will not depend on anything having to do with the comet — a perfect experiment and one that is unlikely to recur soon[9].

To investigate the dynamical response to comet impacts, we ran simulations with the Explicit Planetary Isentropic-Coordinate (EPIC) atmospheric model for Jupiter[10], which is based on the finite-difference algorithm of Hsu and Arakawa[11]. To resolve Jupiter's nonlinear dynamics, our horizontal resolution is 512×256 cells, equivalent to $0.^{\circ}7$ or ∼900 km at the equator. Five active layers simulate

the atmosphere (see Fig. 1), and a sixth layer with a steady wind profile models the interior. Specifying the initial wind in each layer is problematic[12]. The Voyager infrared observations and the thermal wind equation[13] indicate that Jupiter's winds decay with height above the cloud tops. How they vary below the clouds is unknown, although we expect the deep interior to rotate with the magnetic field. In the simulations presented here, we constructed the initial wind field in each active layer by multiplying the observed cloud-top zonal wind[14] by a gaussian function in altitude centered at 500 mbar with a width parameter $\sigma = 2$ pressure scale heights. We set the interior profile to half the cloud-top winds. The choice of interior wind affects planetary-scale (Rossby) waves but does not significantly affect inertia-gravity waves, which are the focus of this work. We gradually force the initial winds for $\sim$50 days to allow the mass and momentum fields to balance. The model then runs without forcing for $\sim$150 days so shear instabilities can develop and equilibrate before the impact perturbation. Fig. 1 here.

EPIC was designed for large-scale meteorological applications and hence incorporates the hydrostatic approximation, which equates the vertical pressure gradient with gravity and ignores vertical accelerations. This unfortunately eliminates sound waves that in the Shoemaker-Levy 9 event may provide seismic information about Jupiter's deep interior[15]. EPIC employs a wave-damping "sponge," gradually introduced in the upper 20% of the layers to prevent reflections from

the top of the model[16]. For these runs only the top layer contains the sponge, but it is nevertheless effective; future work will use more layers. A low-pass filter at the poles prevents numerical instabilities resulting from the small grid spacing.

The impact velocity is well-established[3] at ∼60 km/s. However, disagreeing estimates of the maximum fragment size (1 – 5 km, refs. 17 and 18) and varying density assumptions (0.2 – 1.0 g/cm^3, refs. 19 and 20) combine to make impact kinetic energy uncertain by a factor of ∼600. Further, no reliable constraint has been placed on the energy fraction that remains in the atmosphere after the non-hydrostatic phase. Models[19−21] of the first minutes after an impact vary greatly in their predictions. Ref. 21 predicts fragment penetration to 100 bars and a gradual release of energy. Ref. 19 predicts explosive vaporization at 10 – 100 mbar, while ref. 20 predicts it at 10 bars. Ref. 20 further predicts a rapid (∼10 km/s) rise of superheated gas that escapes the atmosphere and then falls back down onto the stratosphere over a range of several thousand kilometers. Since there are ∼20 fragments of various brightnesses, we expect a range of actual impact altitudes and energies.

To bracket these uncertainties, we modeled heat deposition in the range of 10^{27}–10^{30} ergs at the predicted impact latitude of 43.°9 south (10^{28} ergs corresponds to a 1-km diameter, 1 g/cm^3 fragment, mass 5×10^{14} g). Our hydrostatic model

cannot handle large vertical accelerations, so we start our simulations well after the rise of gas by adding heat to a single layer instantaneously. The heat is spread over as small a disc as possible without violating the hydrostatic assumption; diameters are a few thousand kilometers. We did not run a 10^{30}-erg stratospheric case because the disc size was unphysically large. Since models of the early event disagree on where the energy will ultimately go, we simulated stratospheric and tropospheric depositions, in the layers spanning 16–69 mbar and 287–1,197 mbar, respectively. Fig. 2 here.

All our simulations show both a set of globally-propagating inertia-gravity waves and a longer-lived vortex at the impact site (see Fig. 2). Vortex behavior depends on local conditions, but in our longest-run case (10^{28} ergs, stratospheric deposition, 36 days) the spot sheared into two components that moved west-northwest and east-southeast. In all simulations inertia-gravity waves travel at $\sim$400 m/s in the stratosphere and slower in the troposphere. There is an antipodal wave crossing, but no single focus of energy because of wave dispersion and Jupiter's oblateness. Because there is less mass and stronger stratification, stratospheric deposition excites stronger waves than tropospheric deposition (see Fig. 1). Table 1 contains each simulation's temperature deviation range. The waves interfere with one another behind the first wavefront, making it difficult to determine the functional form of the increase of ΔT with comet energy, although it is not faster than linear.

Table 1 here.

Observers can probe different atmospheric levels by selecting wavelengths that are sensitive to different regions. The predicted temperature deviations caused by Shoemaker-Levy 9 inertia-gravity waves bracket the detection threshold for thermal infrared imaging, which probes the stratosphere[22–24]. Transient condensation effects similar to those seen in mountain lee waves may be visible in high-resolution, reflected-light images of the waves' horizontal passage through the ammonia clouds (upper troposphere). Whether such effects are indeed seen will depend upon local circumstances and the size of the wave. Inertia-gravity waves will be distinguishable from seismic waves[15] by the former's slower propagation rate and stronger thermal signature. In all cases, techniques that take advantage of the waves' circular coherence (see Fig. 2), such as averaging in radial bins around the impact locations, will improve the signal-to-noise ratio of the wave trace. Because of the uniqueness of this event and the potential for significant improvements in dynamical modeling, observers should attempt to determine inertia-gravity wave speeds at as many pressure levels as possible. □

1. Nakano, S. *IAU Circ. No. 5800* (1993).

2. Carusi, A., and Yeomans, D. K. *IAU Circ. No. 5807* (1993).

3. Yeomans, D. K., and Chodas, P. *Bull. Amer. Astron. Soc.* **25,** 1042–1043 (1993).

4. Conrath, B. J., Gierasch, P. J., and Nath, N. *Icarus* **48,** 256–282 (1981).

5. Dowling, T. E., and Ingersoll, A. P. *J. Atmos. Sci.* **46,** 3256–3278 (1989).

6. Ingersoll, A. P., and Cuong, P. G. *J. Atmos. Sci.* **38,** 2067–2076 (1981).

7. Marcus, P. S. *Nature* **331,** 693–696 (1988).

8. Williams, G. P., and Wilson, R. J. *J. Atmos. Sci.* **45,** 207–241 (1988).

9. Melosh, H. J., and Schenk, P. *Nature* **365,** 731–733 (1993).

10. Dowling, T. E. *Bull. Amer. Astron. Soc.* **25,** 1031 (1993).

11. Hsu, Y.-J. G., and Arakawa, A. *Monthly Weather Rev.* **118,** 1933–1959 (1990).

12. Dowling, T. E. *J. Atmos. Sci.* **50,** 14–22 (1993).

13. Pirraglia, J. A., Conrath, B. J., Allison, M. D., and Gierasch, P. J. *Nature* **292,** 677–679 (1981).

14. Limaye, S. S. *Icarus* **65,** 335–352 (1986).

15. Marley, M. S. *Bull. Amer. Astron. Soc.* **25,** 1043 (1993).

16. Klemp, J. B., and Lilly, D. K. *J. Atmos. Sci.* **35,** 78–107 (1978).

17. Scotti, J. V., and Melosh, H. J. *Nature* **365,** 733–735 (1993).

18. Weaver, H. A., Feldman, P. D., A'Hearn, M. F., Arpigny, C., Brown, R. A., Helin, E. F., Levy, D. H., Marsden, B. G., Meech, K. J., Larson, S. M., Noll, K. S., Scotti, J. V., Sekanina, Z., Shoemaker, C. S., Shoemaker, E. M., Smith, T. E., Storrs, A. D., Yeomans, D. K., and Zellner, B. *Bull. Amer. Astron. Soc.* **25,** 1042 (1993).

19. Sekanina, Z. *Science* **262,** 382–387 (1993).

20. Zahnle, K., Mac Low, M.-M., and Chyba, C. F. *Bull. Amer. Astron. Soc.* **25,** 1043 (1993).

21. Ahrens, T. J., Takata, T., and O'Keefe, J. D. *Bull. Amer. Astron. Soc.* **25,** 1043 (1993).

22. Deming, D., Mumma, M. J., Espenak, F., Jennings, D. E., Kostiuk, T., Wiedemann, G., Loewenstein, R., and Piscitelli, J. *Astrophys. J.* **343,** 456–467 (1989).

23. Gezari, D. Y., Mumma, M. J., Espenak, F., Deming, D., Bjoraker, G., Woods, L., and Folz, W. *Nature* **342,** 777–780 (1989).

24. Orton, G. S., Friedson, A. J., Caldwell, J., Hammel, H. B., Baines, K. H., Bergstralh, J. T., Martin, T. Z., Malcom, M. E., West, R. A., Golisch, W. F., Griep, D. M., Kaminski, C. D., Tokunaga, A. T., Baron, R., and Shure, M. *Science* **252,** 537–542 (1991).

ACKNOWLEDGEMENTS. We thank Edward Charrette and the MIT Earth Resources Laboratory for programming assistance and use of their nCUBE 2 massively parallel computer. Work funded by the NASA Planetary Atmospheres program.

Fig. 1 (upper right) The initial temperature *vs.* pressure, *T(p)*, curve for the model atmosphere, showing the tropopause at $\sim$100 mbar. We used the available Voyager data for pressures less than 700 mbar. For higher pressures we extrapolated as shown assuming a slightly stable atmosphere. Such guesswork will be unnecessary if inertia-gravity wave speeds are measured in the troposphere.

(other plots) Temperature deviation profiles for comet-Jupiter impact simulations. The five vertically-stacked profiles in the seven plots correspond to layer interfaces in the model. The top layer extends to zero pressure and the steady-wind interior begins at 5,000 mbar. They show temperature deviations from an unperturbed model one day (light line) and two days (heavy line) after the impact of a comet fragment. Minor ticks on the vertical axis are 0.1 K. Energy deposition altitudes are indicated by the placement of the log of the impact energy in ergs. To determine interface pressure levels (and hence layer spacings), extend the zero of the vertical scale to the pressure axis of the *T(p)* plot. The region close to the impact point is masked for clarity. A low-pass filter removed grid-scale noise.

Fig. 2 (**A**) Simulation of Jupiter's atmosphere one day (24 hours) after impact of a comet fragment. (**B**) Same simulation two days after impact. 10^{28} ergs were deposited in the layer spanning 16–69 mbar (stratospheric deposition); the 69-mbar pressure level is shown here. Height variations on the spheres correspond to changes in pressure, whereas color corresponds to potential vorticity and indicates material initially at the same latitude. Inertia-gravity waves propagate outward from the impact site. The wave propagation rate is determined by the deformation radius, a key dynamical parameter that is uncertain in the troposphere. The circular coherence of the waves even after several days will facilitate detection of relatively small temperature fluctuations.

Editor: Use color slides from original submission, oriented to match these figures.

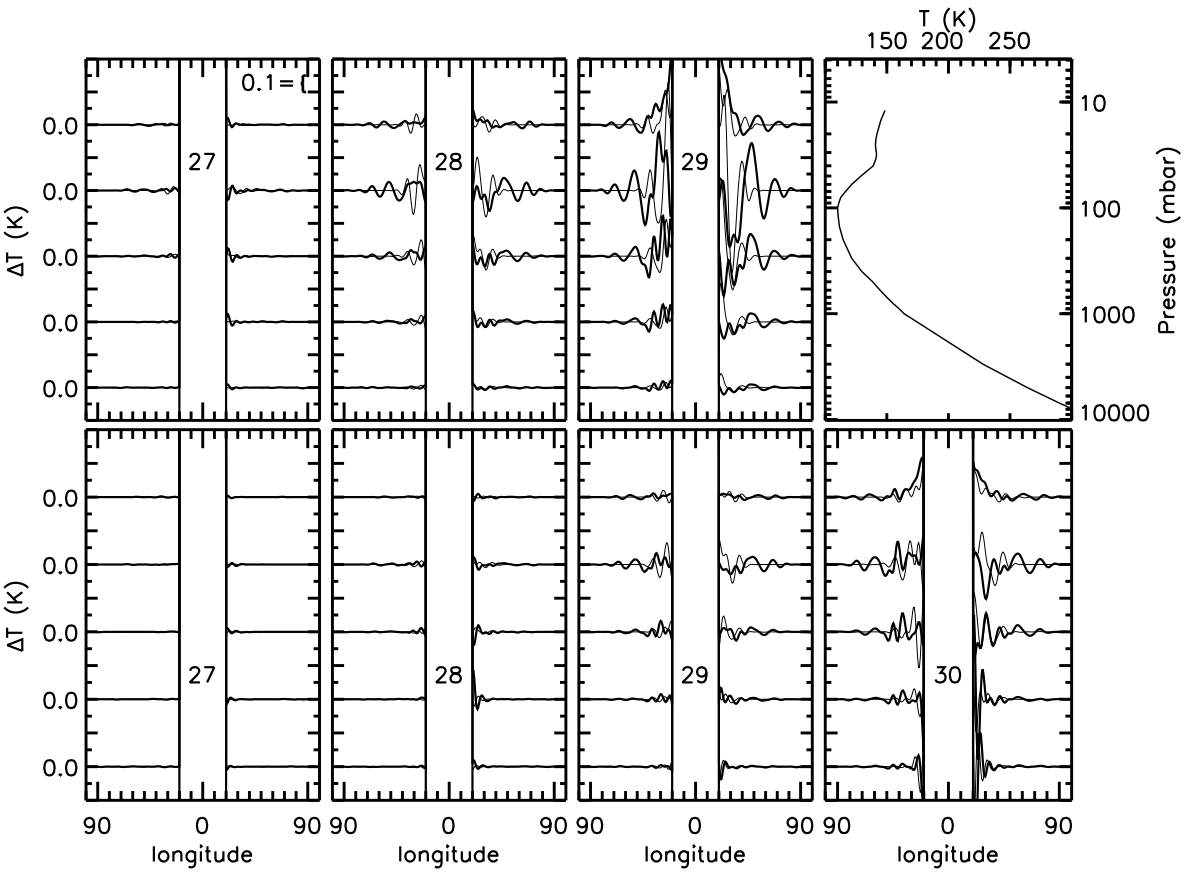
T (K)
150 200 250
0.1 = (
27
28
29
30
ΔT (K)
0.0
10
100
1000
10000
Pressure (mbar)
90 0 90
longitude

A 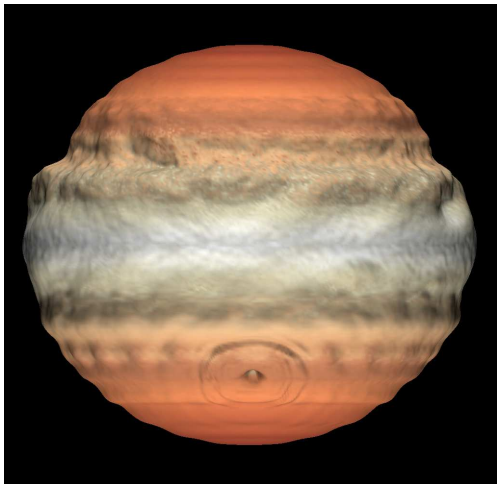

B 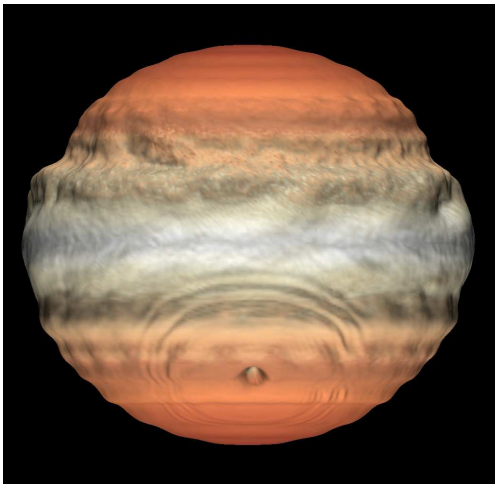

Table 1
Ranges of zonal temperature deviation profiles.

Stratospheric energy deposition (16–69-mbar layer)

	10^{27} ergs		10^{28} ergs		10^{29} ergs	
pressure (mbar)	day 1 ΔT (K)	day 2 ΔT (K)	day 1 ΔT (K)	day 2 ΔT (K)	day 1 ΔT (K)	day 2 ΔT (K)
16	0.02	0.06	0.1	0.1	0.4	0.6
69	0.04	0.09	0.4	0.2	1.2	0.7
287	0.02	0.08	0.2	0.1	0.7	0.5
1,197	0.009	0.07	0.1	0.1	0.3	0.2
5,000	0.004	0.03	0.04	0.04	0.1	0.08

Tropospheric energy deposition (287–1,197-mbar layer)

	10^{27} ergs		10^{28} ergs		10^{29} ergs		10^{30} ergs	
pressure (mbar)	day 1 ΔT (K)	day 2 ΔT (K)	day 1 ΔT (K)	day 2 ΔT (K)	day 1 ΔT (K)	day 2 ΔT (K)	day 1 ΔT (K)	day 2 ΔT (K)
16	0.004	0.02	0.01	0.04	0.07	0.04	0.3	0.3
69	0.009	0.02	0.04	0.07	0.3	0.1	0.4	0.4
287	0.009	0.03	0.04	0.1	0.2	0.1	0.5	0.3
1,197	0.01	0.04	0.06	0.2	0.06	0.1	0.3	0.9
5,000	0.007	0.02	0.02	0.05	0.1	0.1	0.7	0.8